Master‘s Thesis

Title

3D Walking of a Bio-inspired Musculoskeletal Quadruped Robot

Supervisor

Professor Kensuke Harada

Author

Ozgur Ege Aydogan(29C21204)

August 17, 2023

Department of Systems Innovation
Graduate School of Engineering Science
Osaka University

Abstract

In this study, it was aimed to apply the walking strategy of a greyhound dog to a bio-inspired musculoskeletal quadruped robot, to perform the 3D walking of the robot, and to determine the effect of the muscle model on the speed of the robot. Focusing on muscle drive pattern and duration of phases in the gait cycle we verified timing of gait phases and pattern of the pneumatic muscles have a crucial role in quadruped robot walking and speed.

First, the bio-inspired musculoskeletal quadruped robot modeled on the greyhound musculoskeletal system is developed to verify whether 3D walking can be realized. Then, the solenoid valve system that supplies the compressed air to the artificial muscles of the robot was controlled by Arduino Dues, and sensor value transmission between the tension sensor and Arduino Dues was performed using CAN communication. The walking emergence system based on the control pattern of the pneumatic artificial muscles is proposed and walking experiments of the quadruped robot are conducted.Various muscle drive patterns and gait cycles were implemented and compared to examine the effect of the muscle drive pattern and gait cycle on the speed of the robot while it performs the 3D walking. As a result of the experiments, it was confirmed that the 3D walking of the quadruped robot can be realized and the speed of the quadruped robot can be increased by adjusting the muscle pattern, decreasing the duration time of stance and swing phases of the gait cycle.

The 3D walking of the quadruped robot was performed and the speed of the bio-inspired musculoskeletal quadruped was increased based on adjustments in muscle drive pattern, and transition conditions of the gait cycle. It was determined that the speed of the quadruped robot increased by decreasing the stance phase duration and the swing phase duration. It was also found that by increasing the stride length and decreasing the step height of the robot, the walking speed of the robot was increased. In addition, it has been suggested that there is a relationship between the tension sensor measurement and the robot speed, depending on the muscle drive pattern and the phase duration of the gait cycle, even when the tension sensor is not directly involved in the robot control. Results obtained in this study are limited to conducting feedforward control due to the setting of the experiments, and the stable walking experiments based on feedback control, such as tension-based or force-based control, will be a future issue.

Acknowledgments

This research was conducted under the supervision of Professor Koh Hosoda, the head of the Adaptive Robotics Laboratory from the Department of System Innovation, Graduate School of Engineering Science, Osaka University.
I would like to express my sincere gratitude to my supervisor and principal investigator, Prof. Koh Hosoda, for his invaluable guidance and insightful commentaries throughout my research progress and master's program.
This research is supported by the Japanese Government (Monbukagakusho: MEXT) Scholarship that is funded by the Ministry of Education, Culture, Sports, Science and Technology of Japan. I am deeply grateful to have the privilege of being nominated by Osaka University as the recipient of the Japanese Government (Monbukagakusho: MEXT) Scholarship grant.
I would like to express my deep gratitude to Associate Professor Masahiro Shimizu, Assistant Professor Takumi Kawabetsu, and Assistant Professor Shunsuke Shigaki for their support and for giving me various advice.
I would like to thank all my labmates, especially PhD students, for the pleasant and informative conversations we had on robotics, academic life, and advanced technologies.
Finally, I immensely thank my family for their constant blessing and support throughout my master's studies.
This research is supported by the Japanese Government (Monbukagakusho: MEXT Scholarship) that funded by the Ministry of Education, Culture, Sports, Science and Technology of Japan.

This thesis marks not only the end of one journey but the beginning of another.

Contents

List of Figures

List of Tables

Chapter 1

Introduction

Quadruped animals are able to walk adaptively in a variety of terrains through neural mechanisms[1], the interaction between the body, the environment, and the brain[2]. Although many researchers have observed the movements and muscle functions of quadruped animals [3],[4], and have investigated the methods by which animals move their legs in a stable manner[5-17], they have not been able to reach a definite conclusion about how adaptive 3D walking occurs. The essential point to adaptive walking in animals is thought to be the generation of rhythms through neural circuits in the spinal cord and their regulation with sensory stimuli from the periphery. Based on this idea, it can be predicted that legged robots will be able to adapt to their surroundings in the same way that biological organisms do. To explore adaptive 3D walking, our approach to developing a compliant bio-inspired quadruped robot and performing experiments on it, avoiding the ethical issues that arise from physically interfering with quadruped animals, is gaining importance.

Several studies have been conducted to implement adaptive walking techniques in quadruped robots using models that mimic the neurological mechanism of quadruped animals [18-27]. Taga et al. [20] proposed a concept of sensorimotor control of legged locomotion based on neurophysiology and nonlinear dynamics. Masuda et al. [21] presented a musculoskeletal quadruped robot with antagonist muscles using an autonomous decentralized motion control system inspired by the spinal reflex system with reciprocal innervation. Moreover, Yamada et al. [24] developed a bio-inspired quadrupedal robot with a nervous system with a spinobulbar system model without predefined gait patterns. Maufroy et al. [25] proposed a generic legged locomotion controller that can incorporate both posture and rhythmic movement controls and regulate phase transitions based on walking speed has been developed. Owaki et al. [28] presented a simple-structured quadruped robot using a

CPG model consisting of four decoupled oscillators with local force feedback in each leg. In addition, Fukuhara et al. [29] developed a CPG model that uses just four discrete oscillators with local force feedback in each leg, adapts effectively to variations in walking speed, and mimics the walking patterns of the quadrupeds. It has been shown in these studies that the walking stability and energy efficiency of legged robots can be improved by autonomous decentralized walking, which adjusts the walking rhythm with sensory inputs from the environment. Since most of the previously proposed quadruped robots have simple leg structures, the load on each leg can be estimated based on the ground reaction force from the ground when walking on flat ground. However, when walking on uneven ground, it should be taken into account that the value of the ground reaction force changes unevenly depending on how the contact with the ground occurs, and it is difficult to properly estimate the load on the legs. Moreover, current quadrupedal robots have difficulty maintaining stable walking. Therefore, it is aimed to perform adaptive 3D walking by developing an adaptive control method that allows the robot to adjust its leg phases during locomotion. Furthermore, inspired by the anatomy of racing greyhounds, it is aimed to capture the essence of natural walking and thus achieve the agile and realistic locomotion of the quadruped robot.

To investigate the mechanism adaptive 3D walking approach, a bio-inspired musculoskeletal quadruped robot is developed that is driven by pneumatic artificial muscles that imitate a racing greyhound. The robot is structured to have 4 links and 7 artificial muscles in each forelimb, and 4 links and 7 artificial muscles in each hindlimb to duplicate the musculoskeletal structure of the greyhound as much as possible. Tension sensors using strain gauges are used to measure the tension applied to the gastrocnemius muscle and carpi extensor muscles in real-time while the robot is walking. Moreover, the walking emergence system based on the control pattern of the pneumatic artificial muscles is realized. In addition, various muscle drive patterns and gait cycles were implemented and compared to examine the effect of the muscle drive pattern and gait cycle on the speed of the robot while it performs the 3D walking.

In this study, the adaptive 3D walking of the compliant quadruped robot was performed. The speed of the bio-inspired musculoskeletal quadruped was increased based on adjustments in muscle drive pattern, and transition conditions of the gait cycle. It was determined that the speed of the quadruped robot increased by decreasing the stance phase duration and the swing phase duration. It was also found that by increasing the stride length and decreasing the step height of the robot, the walking speed of the robot was increased. In addition, it has been suggested that there is a relationship between the

tension sensor measurement and the robot speed, depending on the muscle drive pattern and the phase duration of the gait cycle, even when the tension sensor is not directly involved in the robot control.

The thesis is organized in such a way that firstly the design of the robot and the reflex-based control system are depicted, then some experimental results of 3D walking with the robot are demonstrated, and finally, our results are discussed.

Chapter 2

Theoretical Background

2.1 Pneumatic Artificial Muscle

Pneumatic artificial muscle (PAM) is an artificial muscle that contracts when air is supplied. It is essentially a rubber tube covered with a plastic knit sleeve. When the air is applied to a rubber tube, it expands in all directions. When the air is applied to the artificial muscle, the radial force pushes the sleeve, and it translates the force to contraction. As a result, when supplied with compressed air, the artificial muscle generates force. The muscle is essentially soft since it includes air. The musculoskeletal system of animals and humans can be realized by employing artificial muscles. The energy source of a PAM is often air [30], which is either pumped into it or removed from it. The actuator is thus driven by the pressure differential between the interior and outside gas.

Pneumatic muscles have several advantages [31] over electric motors, shape memory alloys (SMA), pneumatic pistons, and hydraulic actuators in various fields such as robotic, medical, aerospace, and industrial applications. PAMs are lightweight, flexible, compliant, adaptable, energy-efficient, safety, and cost-effective. Moreover, they provide a safe human-robot interaction, a high power-to-weight ratio, natural-like movement, and biomechanical Compatibility. Various artificial muscles [32] including McKibben muscle, pleated muscle, Kevlar fiber reinforced artificial muscle, Yarlott Reticulated muscle, Paynter Hyperboloid muscle, and ROMAC muscle are shown in Fig.2.1

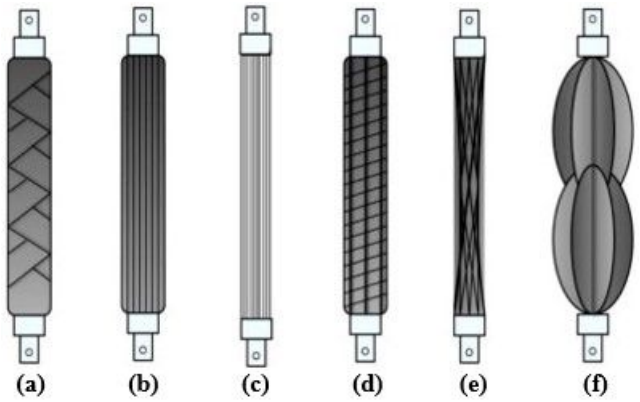

Figure 2.1: Conventional PAMs (a) McKibben Muscle/Braided Muscle; (b) Pleated Muscle; (c) PAM reinforced by Kevlar Fiber; (d) Yarlott Netted Muscle; (e) Paynter Hyperboloid Muscle; (f) ROMAC Muscle

Chapter 3

Materials and Method

3.1 Musculoskeletal Quadruped Robot

3.1.1 Robot Overview

In this study, the bio-inspired musculoskeletal quadrupedal robot previously developed in our lab has been redeveloped by redesigning the leg structure, leg links, and joint mechanisms and re-adjusting the moment arms of its muscles to increase walking stability and realize 3D walking. The skeletal structure robot's legs were redesigned in Autodesk Inventor, which is shown in Fig.3.1. The robot is developed based on the functional anatomy and muscle structure of a greyhound's musculoskeletal structure [33]-[35]. In the robot, aluminum pipes are used for the skeletal structure, and McKibben-type pneumatic artificial muscles (MPA) are used for the actuators. Design parameters of the quadruped robot and their values are represented in Table 3.1. The appearance of the musculoskeletal quadruped robot is shown in Fig.3.2. Moreover, the side view and top view of the musculoskeletal robot are shown in Fig.3.3 and Fig.3.4. The design parameters of the robot such as length, width, height, and weight are 1000 mm, 420 mm, 600 mm high, and 12 kg, respectively. The spine, shoulders, and hips are rigid bodies, and all of them are angled at 150 degrees. The forelimb has three corresponding links corresponding to the humerus, forearm, and carpal bones, and each link length is 200 mm for the humerus, 235 mm for the forearm, and 165 mm for the carpal. On the other hand, the hindlimb has three corresponding links to the femur, crus, and tarsal bone, and the length of each link is 210 mm for the femur, 293 mm for the crus bone, and 145 mm for the tarsal bone.

Figure 3.1: CAD Design of the Skeletal Structure

Parameter	Value
Length x Width x Height $[mm]$	1000 x 420 x 600
Total weight $[kg]$	12
Forelimb weight $[kg]$	6.3
Hindlimb weight $[kg]$	5.7
Number of muscles	30

Table 3.1: Design parameters of the quadruped robot

3.1.2 Musculoskeletal Structure

The musculoskeletal structure of the robot is demonstrated in Fig.3.5 The forelimb of the robot has a total of 7 muscles, including 4 mono-articular muscles, and 3 bi-articular muscles. According to muscle functions, latissimus dorsi (LD), supraspinatus (SS), triceps brachii (TBlm), and flexor carpi ulnaris (FCU) are selected as mono-articular muscles of the forelimbs, while biceps brachii (BB), triceps brachii (long) (TB), and extensor carpi radialis (ECR) are selected as bi-articular muscles of the forelimbs. The name, length, and function of each muscle used in the forelimb muscle structure of the robot are represented in Table 3.2 On the other hand, the hindlimb of the robot has a total of 8 muscles, including 5 mono-articular muscles, and 3 bi-articular muscles. According to muscle functions, iliopsoas (IP), gluteus maximus (GL), vastus lateralis (VL), tibialis anterior (TA), and soleus (SOL) are selected as mono-articular muscles of the hindlimb, while rectus femoris (RF), biceps femoris (BF), and gastrocnemius (GA) are selected as

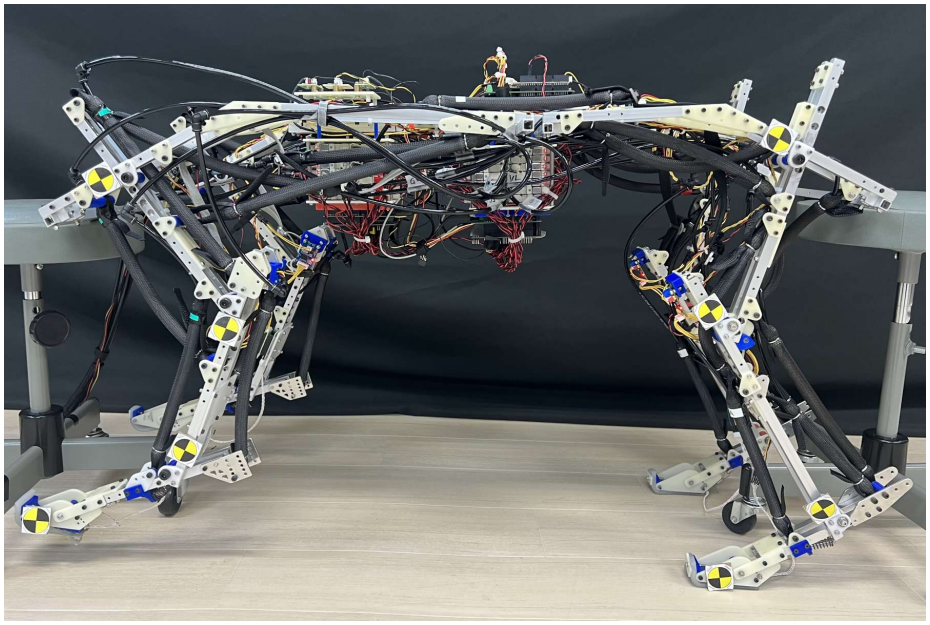

Figure 3.2: The appearance of the musculoskeletal quadruped robot

bi-articular muscles of the hindlimb. The name, length, and function of each muscle used in the hindlimb muscle structure of the robot are represented in Table 3.3 The moment arm length of each muscle of the quadruped robot is represented in Fig.3.6 in mm. The musculoskeletal structure is designed to be simplified as each leg joint can only move in the sagittal plane.

Muscles	Length $[mm]$	Function of muscles
latissimus dorsi (LD)	300	shoulder flexion
supraspinatus (SS)	275	shoulder extension
biceps brachii (BB)	210	shoulder extension, elbow flexion
triceps brachii(long) (TB)	210	shoulder flexion, elbow extension
triceps brachii (TBlm)	230	elbow extension
extensor carpi radialis (ECR)	180	elbow flexion, wrist flexion
flexor carpi ulnaris (FCU)	200	wrist extension

Table 3.2: Name, length, and function of each muscle of the forelimb

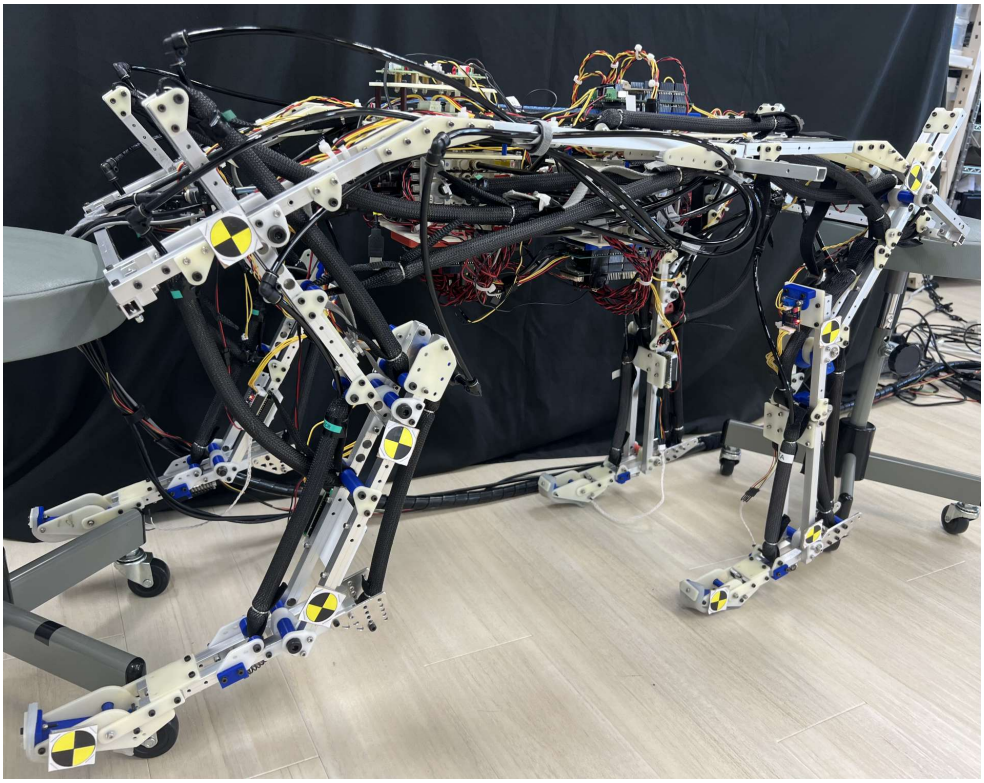

Figure 3.3: The side view of the musculoskeletal quadruped robot

3.1.3 McKibben-type pneumatic artificial muscles

In this study, McKibben-type pneumatic artificial muscles are used as actuators of the system. In this study, McKibben-type pneumatic artificial muscles (MPAs) are used as actuators of the system. This soft actuator has a two-layer structure in which a rubber tube is covered with a nylon sleeve and when compressed air is supplied to the rubber tube, it shrinks by a maximum of about 20 percent as represented in Fig. 3.7 High precision control is difficult for MPAs because of their non-linear behavior characteristics such as air compressibility and hysteresis. On the other hand, the rigidity of the joints can be adjusted by arranging them antagonistically with respect to the joints of the robot due to the flexibility of the actuators as shown in Fig.3.8 Joint behavior and joint stiffness can be adjusted by arranging MPA antagonistically for each joint in the robot developed in this study. The expansion and the contraction lengths are determined by internal pressure and at the same time the elasticity of the muscle changes. When both the left and right muscles are relaxed, the neutral position is maintained and the stiffness of the joint is low. When air is supplied to both the left and right muscles,

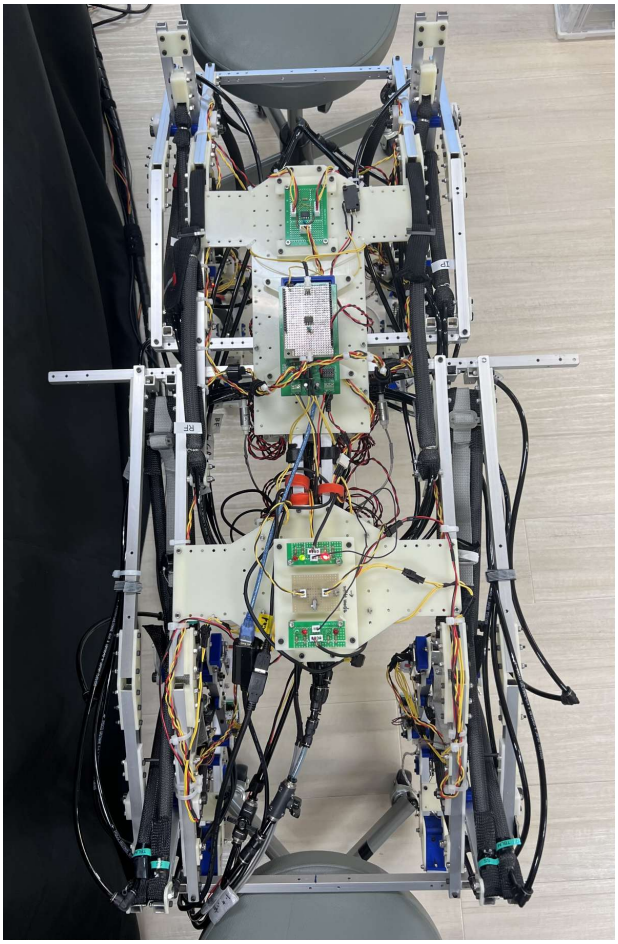

Figure 3.4: The top view of the musculoskeletal quadruped robot

the neutral position is similar to the condition that both the left and right muscles are relaxed, but the joint stiffness is high. When only the left or right muscle muscle is supplied with air, the joint bends, and the joint angle and joint stiffness change due to the internal pressure of the muscle The joint angle and stiffness can be changed by adjusting the internal pressure of the muscles on both sides. McKibben-type pneumatic artificial muscle is excellent in mimicking the musculoskeletal structure of living organisms due to the ease of stiffness adjustment and the similarity of the length-load curve to that of living muscle. McKibben-type pneumatic artificial muscles were placed antagonistically with respect to the joint to reproduce the leg structure of the racing greyhound.

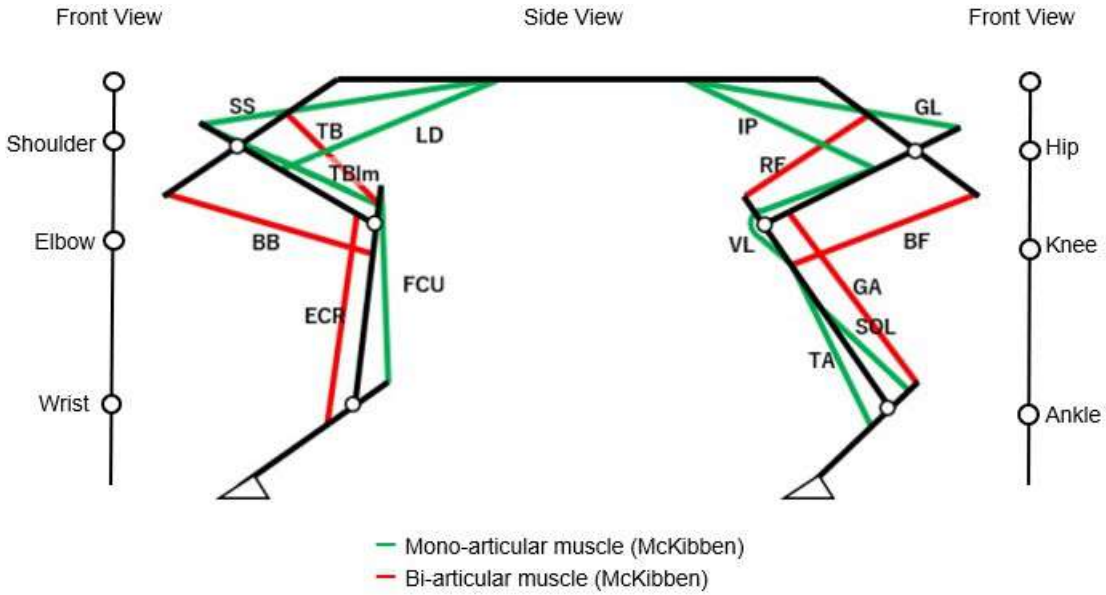

Figure 3.5: The musculoskeletal structure of the robot. The green line is the mono-articular muscle, and the red line is the bi-articular muscle.

3.2 Sensor Configuration

3.2.1 Tension Sensor

The tension sensor with strain gauges, which is shown in Fig.3.9, is used to obtain the tension of the gastrocnemius and carpi extensor muscles during walking. Four tension sensors that were developed in our laboratory, are connected between the robot's leg links and its MPAs as shown in Fig.3.10, to measure the tension applied to each muscle in real-time during the movement of the robot. In order to obtain the tension sensor's value with Arduino, the sensor is connected to the Arduino via the extension board. The expansion board for the tension sensor is not powered by the Arduino, but it connects an ATX power supply separately to provide a stable power supply. Since the sensor value of the tension sensor drifts for several minutes after starting to read, a few minutes were waited after acquiring the sensor value during the experiment before starting to read the value. The tension sensor is attached to the ankle joint extensor muscles, which are the extensor carpi ulnaris (FCU) muscle in the forelimb, and soleus (SOL) muscle in the hindlimb.

Muscles	Length $[mm]$	Function of muscles
iliopsoas (IP)	250	hip flexion
gluteus maximus (GL)	250	hip extension
biceps femoris (BF)	250	hip extension, knee flexion
rectus femoris (RF)	200	hip flexion, knee extension
vastus lateralis (VL)	180	knee extension
gastrocnemius (GA)	250	knee flexion, ankle flexion
tibialis anterior (TA)	160	ankle flexion
soleus (SOL)	110	ankle extension

Table 3.3: Name, length, and function of each muscle of the hindlimb

3.3 Control System Configuration

Since the relation between adaptive walking and muscle drive pattern and robot speed and gait cycle are investigated in this study, the feedforward control method is used to perform precise trajectory tracking and rapid control response. The control system configuration of the artificial muscles is demonstrated in Fig.3.11 Compressed air supplied to each muscle was supplied from an external compressor, and the pressure was set to 0.6 [Mpa] by a regulator. Compressed air is supplied to each MPA through a solenoid valve, and air supply (ON), exhaust (OFF), and closing (CLOSE) are selected by opening and closing the solenoid valve of the valve. SMC's VQZ1321-6L1-C6 is used for the solenoid valve. The opening and closing operation of the solenoid valve is performed by Arduino Due, which is shown in Fig.3.12 To control the solenoid valves, an extension board is attached to the Arduino Due and each valve is operated. Due to the limited number of pins on the expansion board, the solenoid valves of the front and rear legs are assigned to separate Arduino Dues. The two Arduino Dues have the same program execution timing by sharing the reset pin. Transmission and reception of each sensor value are performed by CAN communication. For CAN communication, the Arduino Due is connected to a CAN transceiver (MCP2551), and the Arduino Nano is connected to a CAN controller (MCP2515). CAN communication has a line-type network structure and was adopted because it is resistant to external noise. The system configuration of CAN communication is represented in Fig.3.13 For solenoid valve control, tension sensors and Arduino Dues are connected by a common CAN bus and information can be exchanged between any node. Furthermore, sensor values are acquired for solenoid valve control, so the sensor node side does not receive information from its CAN communication. In addition, during the experiment, each sen-

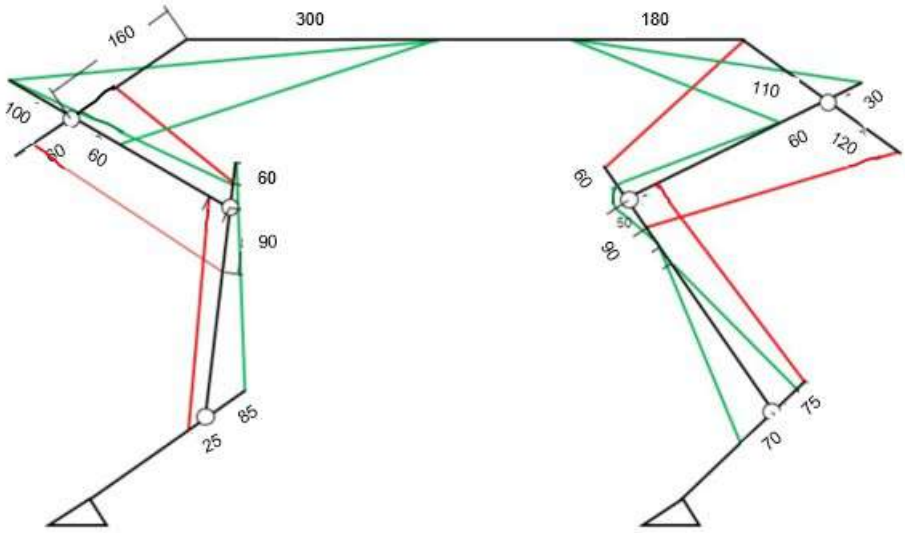

Figure 3.6: The moment arm length of each muscle of the robot.

sor data is acquired from the Arduino Due on the forelimb for data analysis by serial communication. The tension sensor is provided with a dedicated Arduino Due, the tension value is used to operate the solenoid valve via CAN communication, and data is sent to Arduino Due at 170Hz. The transmission and reception of each sensor value synchronize the reception timing by setting a flag in the control code and updating the sensor value.

3.4 Walking Emergence Based on Muscle Drive Pattern

In this study, in order to investigate the effects of muscle drive patterns on quadruped walking, the walking emergence system based on the control pattern of the pneumatic artificial muscles is proposed. The muscle drive pattern regulates the activation of muscles that move the joints of the musculoskeletal robot. The forces required to move the limbs and drive the robot forward are generated by proper activation. The muscle drive pattern controls the time and sequencing of muscle activations, which is essential for walking. In addition, the muscle drive pattern affects the coordination of the robot's gait. Considering the stated characteristics of the muscle drive model, I hypothesized that the phase durations of the gait cycle, especially the stance and swing phases, and the muscle drive pattern play a crucial role in determining the robot's walking speed. I suggested that variations in the muscle drive

Figure 3.7: Natural state (top) and air-supplied state (bottom) of McKibben-type pneumatic artificial muscle

pattern and gait cycle phase duration control the speed of the robot by adjusting the frequency and intensity of muscle activations, which is crucial for achieving different walking speeds. The muscle drive pattern of each phase was determined by considering the walking pattern studies by Nakatsu et al [36], [37] and Ekeberg et al. [38]. In addition, Based on electromyograms [39], [40] in canine walking, the role of each muscle was evaluated. The muscle drive patterns and transition conditions in each state of the forelimb and hindlimb gait cycle are demonstrated in Fig.3.14 and Fig.3.15, respectively.

The gait cycle of each leg is set up into stance, lift-off, swing, and touch-down, which is represented in Fig.3.14 and Fig.3.15, for the forelimb and hindlimb, respectively. For the forelimb gait cycle, in the stance phase, the latissimus dorsi (LD), supraspinatus (SS), triceps brachii longus (TB), triceps brachii (TBlm), and flexor carpi ulnaris (FCU) are contracted during the stance phase. The latissimus dorsi (LD), triceps brachii (TB), triceps brachii (TBlm), and flexor carpi ulnaris (FCU) are stimulated in the lift-off phase. After that, the latissimus dorsi (LD), biceps brachii (BB), and extensor carpi radialis (ECR) muscles in the swing phase drive the supraspinatus (SS), triceps brachii (TBlm), triceps brachii longus (TB), and flexor carpi ulnaris (FCU), during the touch-down phase.

For the hindlimb gait cycle, in the stance phase, gluteus maximus (GL), biceps femoris (BF), rectus femoris (RF), vastus lateralis (VL), soleus (SOL),

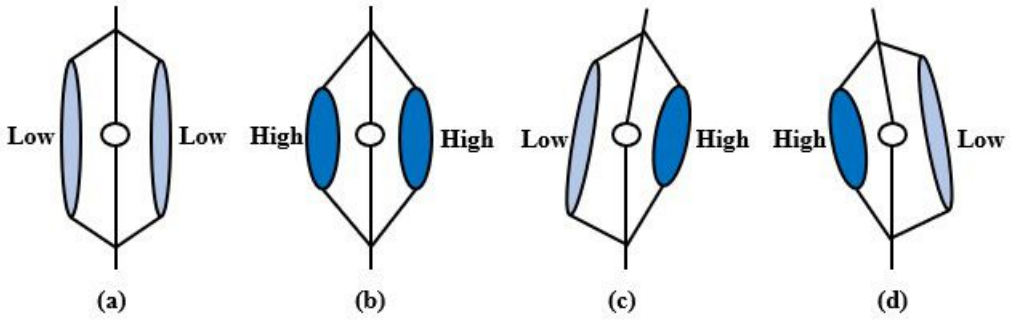

Figure 3.8: Antagonistic placement of pneumatic artificial muscles. (a)When both the left and right muscles are relaxed. (b)When air is supplied to both the left and right muscles. (c),(d) When only the left or right muscle muscle is supplied with air.

Figure 3.9: The control system configuration of the robot. The red line indicates transmission from the tension sensor, the blue line indicates the supply and exhaust of compressed air, and the green dotted line indicates the transmission of sensor data to the PC.

tibialis anterior (TA), and gastrocnemius (GA) are contracted. Then, during the lift-off phase, gluteus maximus (GL), vastus lateralis (VL), soleus (SOL), tibialis anterior (TA), and gastrocnemius (GA) are stimulated. After that, iliopsoas (IP) during swing phase. , biceps femoris (BF), tibialis anterior (TA), iliopsoas (IP), biceps femoris (BF), and tibialis anterior (TA) muscles in the swing phase drive iliopsoas (IP), biceps femoris (BF), vastus lateralis (VL), gastrocnemius (GA), soleus (SOL), and tibialis anterior (TA) muscles, during the touch-down phase.

In order to analyze the speed of the robot in the conditions performed depending on different muscle models and phase states, shoulder joint analysis was performed with the data obtained from the real-time video of the robot in the Kinovea program.

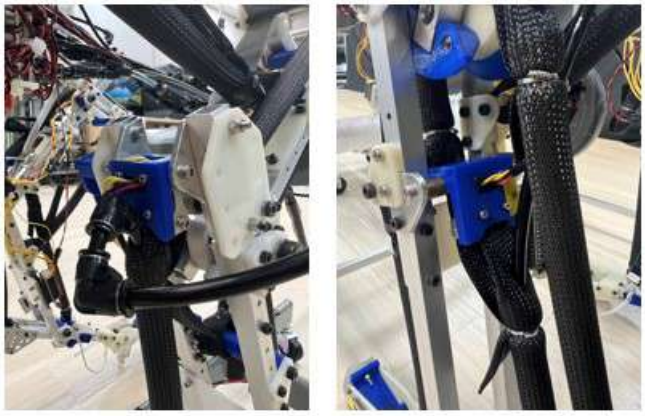

Figure 3.10: The control system configuration of the robot. The red line indicates transmission from the tension sensor, the blue line indicates the supply and exhaust of compressed air, and the green dotted line indicates the transmission of sensor data to the PC.

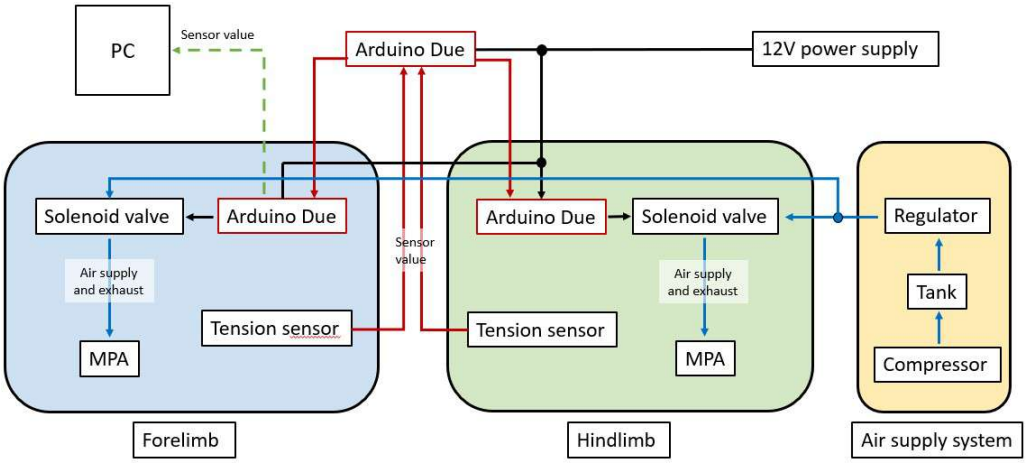

Figure 3.11: The control system configuration of the robot. The red line indicates transmission from the tension sensor, the blue line indicates the supply and exhaust of compressed air, and the green dotted line indicates the transmission of sensor data to the PC.

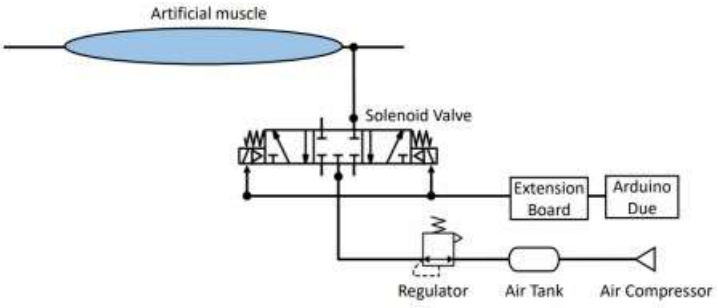

Figure 3.12: The control system configuration of the artificial muscles.

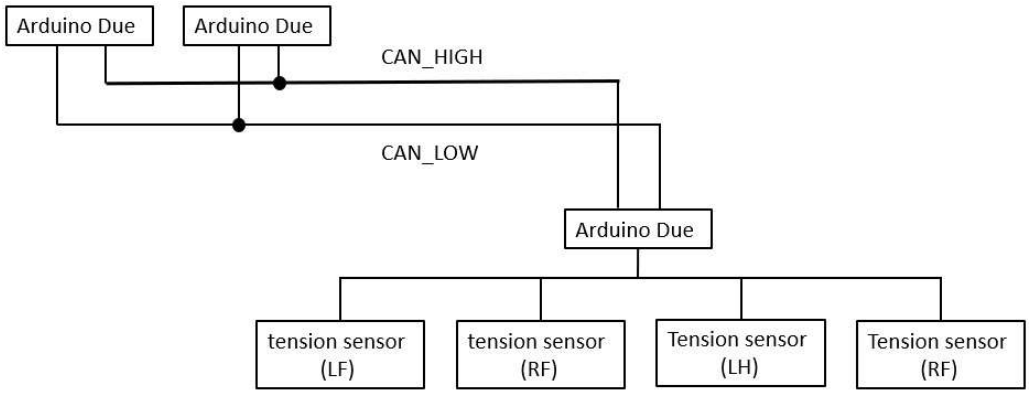

Figure 3.13: The configuration of CAN communication. LF, RF, LH, and RH denote sensors for the left front leg, right front leg, left hind leg, and right hind leg, respectively. All nodes share a common bus.

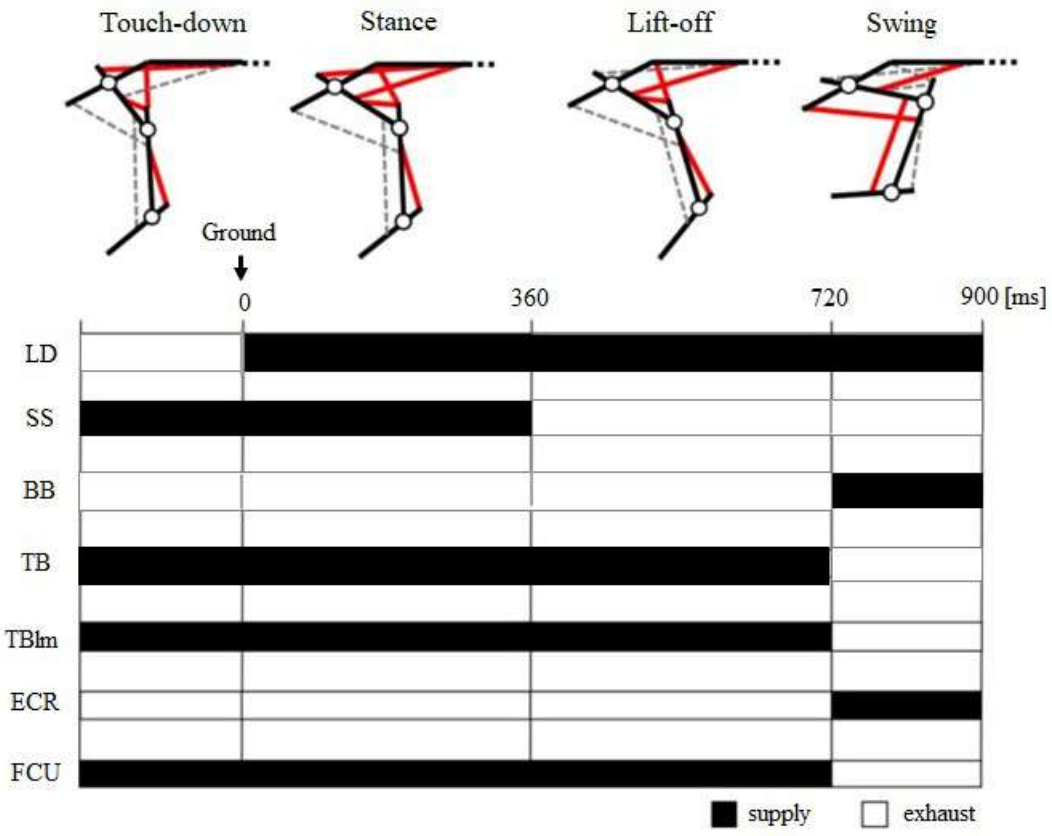

Figure 3.14: The muscle drive patterns and transition conditions in each state of the forelimb gait cycle. In each state, active muscles are indicated by red lines and inactive muscles by dotted lines.

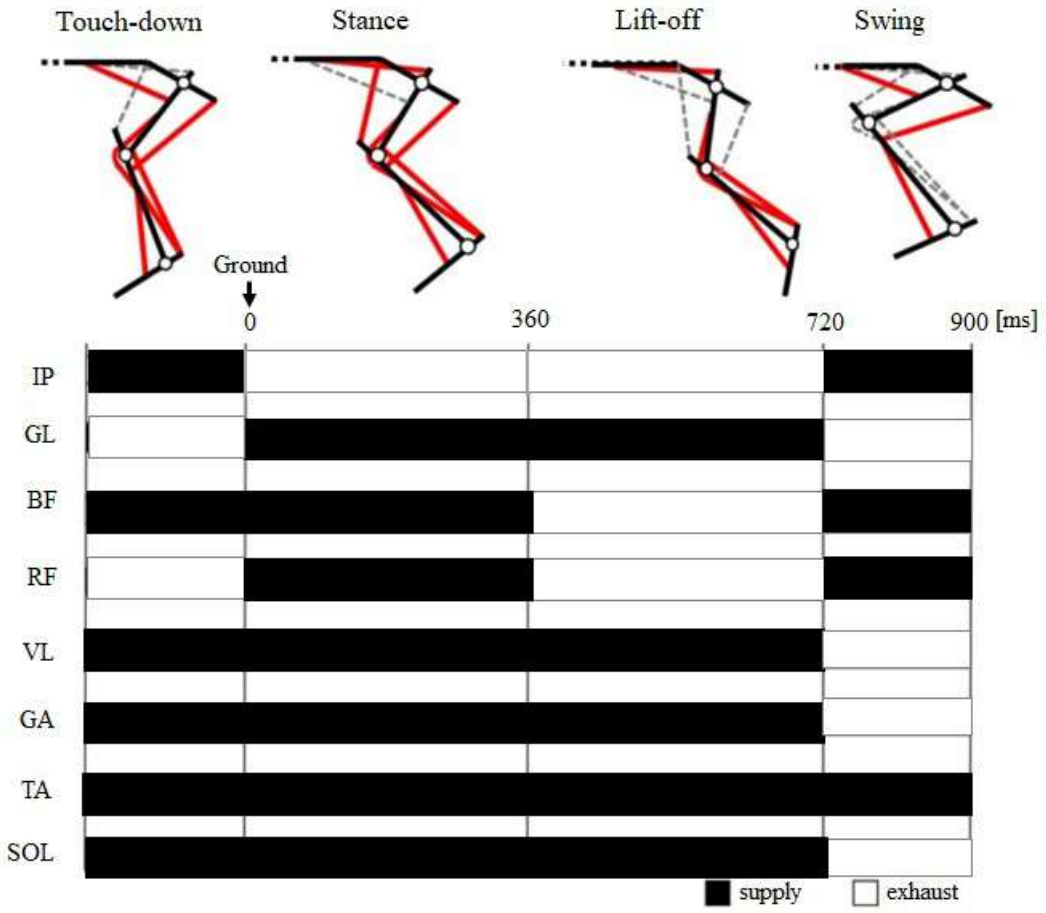

Figure 3.15: The muscle drive patterns and transition conditions in each state of the hindlimb gait cycle. In each state, active muscles are indicated by red lines and inactive muscles by dotted lines.

Chapter 4

Experiments

4.1 Walking Experiments

4.1.1 Experimental Environment

The proposed method, which is the walking emergence of the bio-inspired musculoskeletal quadruped robot based on muscle drive pattern, is verified by walking experiments. Walking experiments are conducted in a laboratory environment on a two-dimensional ground along a fixed 2-meter experiment path shown in Fig.4.1 During the experiments, the two-dimensional holding system with the rotating part and the wheel part shown in Fig.4.2 was fixed to the body of the robot. The upper part of the wheel part is connected to the slide part of the rotating part, and the wheel is moved back and forth on the guide frame. The rotating part and the slider part allow the rotation and vertical movement of the robot's trunk in the pitch direction, and the movement of the wheel part is restricted only in the front-back direction on the guide frame so that the robot's trunk can be moved. By placing it on the guide frame, only forward and backward movement is allowed, and rotational direction is restricted. The experimental conditions were inspired by the experiment conducted by Raibert et al. [42]. In addition, the initial phase of each control is given as a trot phase. The threshold values used for ground contact judgment for each of the tension sensors are shown in Table 4.1.

4.1.2 Experiments Based on Muscle Drive Patterns and Gait Cycle Phase Durations

In walking experiments, experiments with different muscle drive patterns and gait cycle phase duration were performed to verify the effects of muscle drive

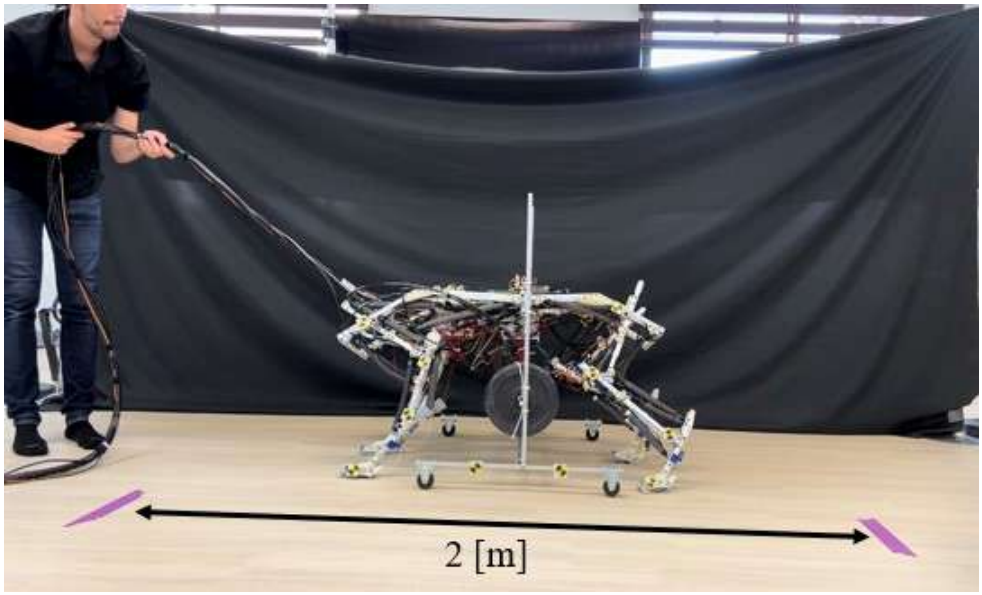

Figure 4.1: Experimental environment for ground walking.

Leg	Threshold $[kg]$
Left forelimb	3.5
Right forelimb	3.5
Left hindlimb	13
Right hindlimb	13.5

Table 4.1: Threshold values used to determine whether the tension sensor is grounded.

patterns on the speed of the robot, as described in the proposed method. Various gait cycle phase durations were implemented to the determined muscle drive pattern, and two main gait cycle phase durations were determined as the experimental conditions. The phase times of these two muscle model conditions are shown in Table 4.1 and Table 4.2. The duration of the stance phase in Gait Cycle-1 was decreased by approximately half in Gait Cycle-2, and the duration of the swing phase in Gait Cycle-1 was decreased by approximately forty percent in gait cycle condition-2. The muscle drive patterns and transition conditions in each state of the forelimb and hindlimb gait cycle of Condition-1 are demonstrated in Fig.4.3 and Fig.4.4, respectively. Moreover, the muscle drive patterns and transition conditions in each state of the forelimb and hindlimb gait cycle of Condition-2 are demonstrated in Fig.4.5 and Fig.4.6, respectively.

Figure 4.2: Two-dimensional restraint system.

Phase	Duration $[ms]$
Touch-down	120
Stance	620
Lift-off	620
Swing	120

Table 4.2: Phase Durations of Gait Cycle Condition-1

Phase	Duration $[ms]$
Touch-down	180
Stance	360
Lift-off	360
Swing	180

Table 4.3: Phase Durations of Gait Cycle-2

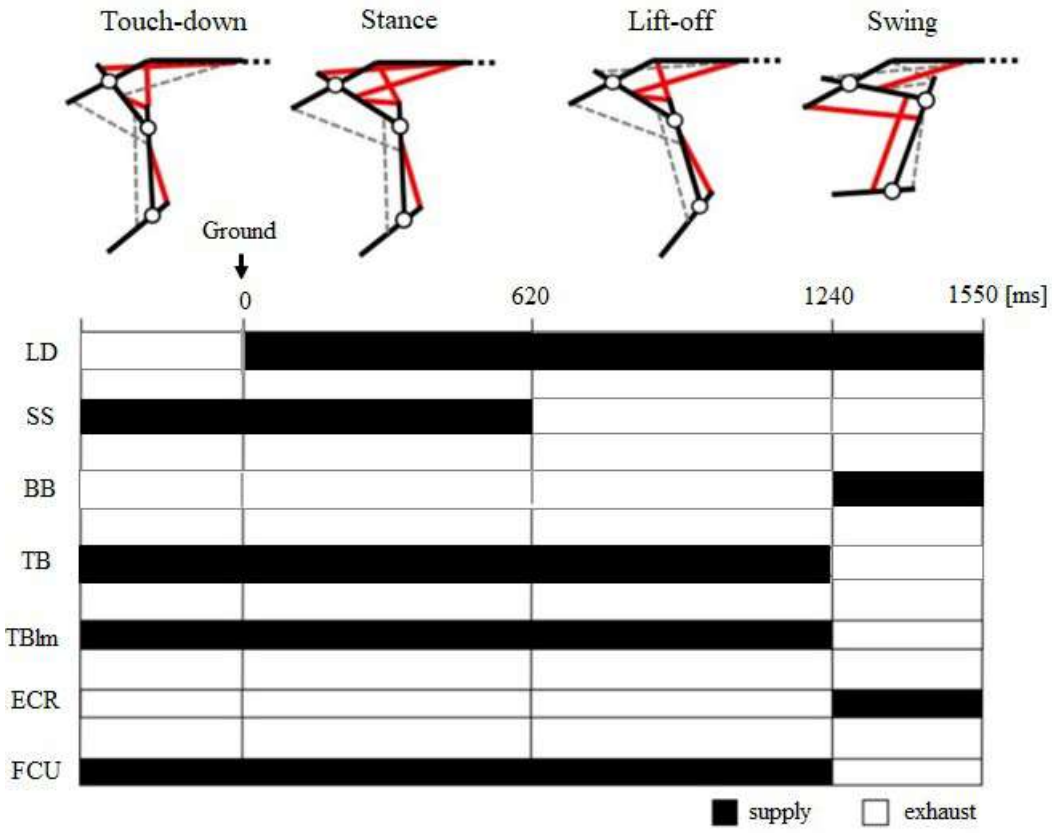

Figure 4.3: The muscle drive patterns and transition conditions in each state of the forelimb gait cycle of Condition-1.

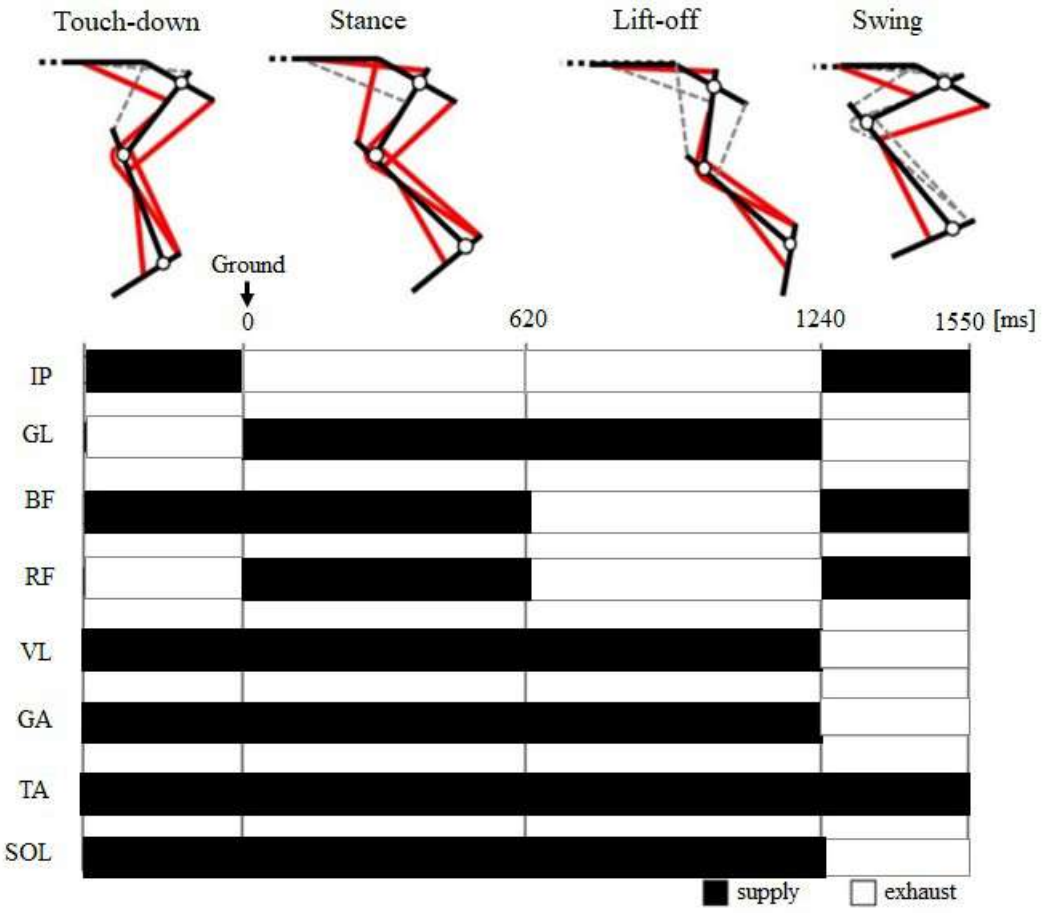

Figure 4.4: The muscle drive patterns and transition conditions in each state of the hindlimb gait cycle of Condition-1.

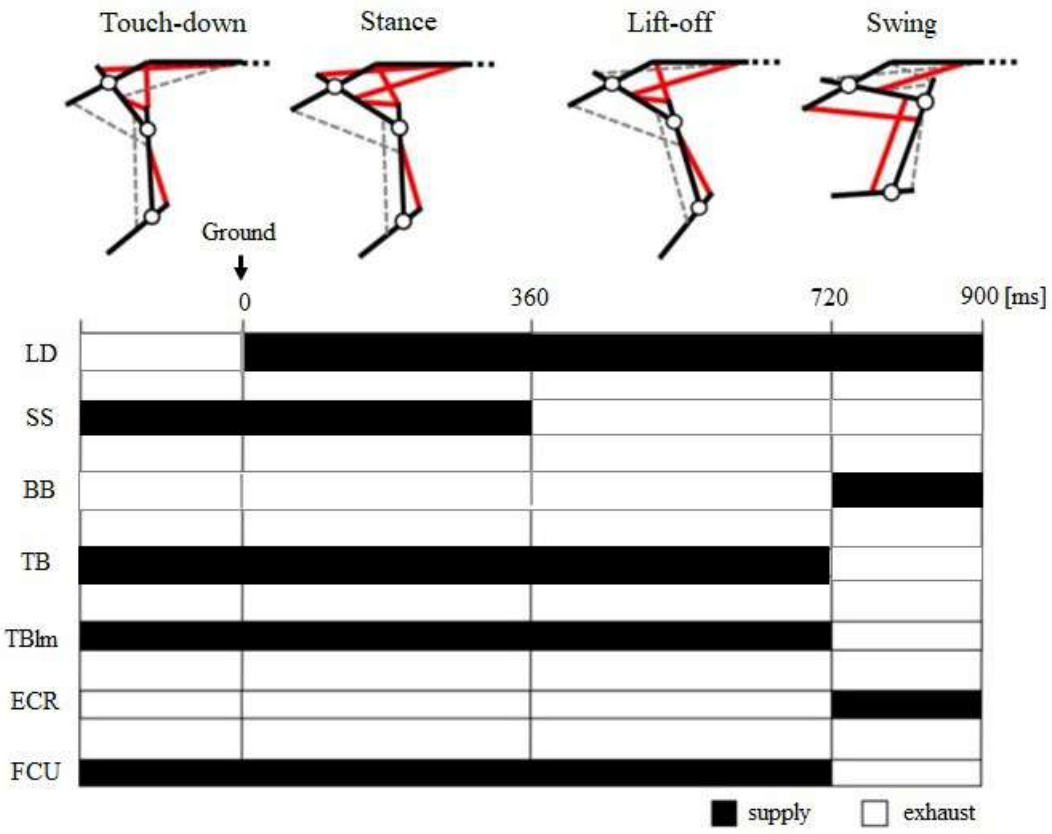

Figure 4.5: The muscle drive patterns and transition conditions in each state of the forelimb gait cycle of Condition-2.

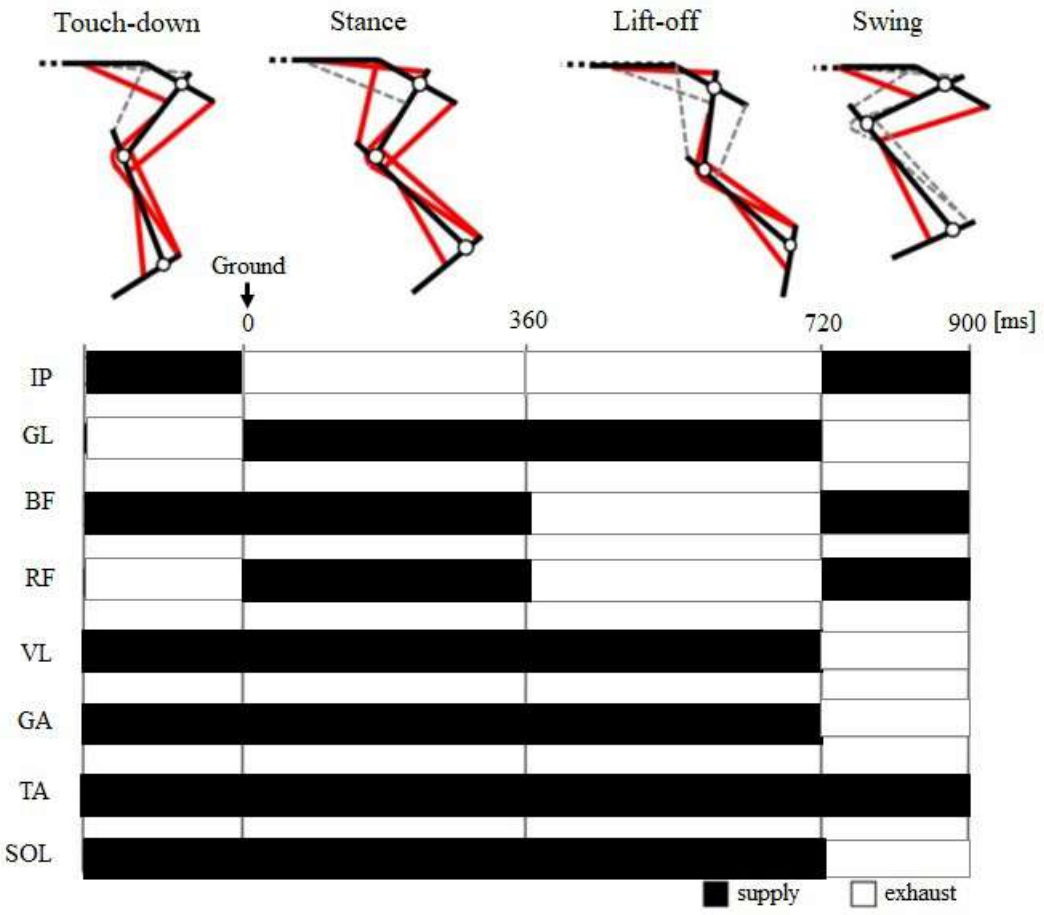

Figure 4.6: The muscle drive patterns and transition conditions in each state of the hindlimb gait cycle of Condition-2.

Chapter 5

Results

5.1 Muscle Drive Pattern and Gait Cycle Phase Duration Based Walking Experiment Results

A snapshot of one cycle of the quadruped robot in the Gait Cycle-1 and Gait cycle-2 experiments are shown in Fig.5.1 and Fig.5.2, respectively.

The values of the quadruped robot speed in Gait Cycle-1 and Gait Cycle-2 experiments, obtained by performing shoulder joint analysis in the Kinovea software, are shown in Fig.5.3. According to the real-time video record, the robot completed the experiment path in 15.4 [s] in the Gait Cycle-1 condition, while it completed the same fixed 2-meter path in 9.2 [s] in the Gait Cycle-2 condition. The speed of the robot in the gait cycle-2 condition and the speed in the gait cycle-1 were found to be 0.11 m/s and 0.20 m/s, respectively. Therefore, the adjustments made to the muscle pattern and the gait cycle enabled the robot to increase its speed almost twice. This proves our hypothesis stated in the proposed method and shows that reducing the duration of the stance phase and swing phase increases the speed of the robot. By reducing the stance phase duration, the robot spent less time on the ground with each leg before going into the swing phase, allowing the robot to reach a higher stride frequency. In addition, by reducing the swing phase duration, the robot spent less time in the air between steps, allowing for quicker transitions to the next step and more forward movement. The stride length values of the robot in Gait Cycle-1 and Gait Cycle-2 conditions are demonstrated in Fig.5.4. According to Fig.5.4, it was found that decreasing the duration time of the stance phase in the gait cycle allowed the legs to travel a greater distance with each stride and increased stride length. Increasing the stride

length generally led to an increase in the robot's walking speed. With each step covering a greater distance, the robot achieved a higher overall speed within a fixed time frame. In addition, it was observed that there is an inverse relationship between stride length and swing phase duration. As the stride length increased, the time spent in the swing phase decreased. Shorter swing phases, linked to longer stride lengths, contributed to faster walking speed. This is because the robot spent less time in the air between steps, allowing for quicker transitions to the next step and more forward movement.

The shoulder joint heights obtained in relation to the shoulder joint trajectories obtained using shoulder joint analysis under the Gait Cycle-1 and Gait Cycle-2 conditions are shown in Fig.5.5. Furthermore, the average values and standard deviation values of the shoulder step height under Gait Cycle-1 and Gait Cycle-2 conditions are shown in Fig.5.6. According to the results of Fig.5.5 and Fig.5.6, the average height of the shoulder joint during movement along the two-meter experiment path in the Gait Cycle-1 experiment was 47 cm, while the average height in the Gait Cycle-2 condition, in which the swing phase was halved, was 45 cm. Based on this result, it was proven that by shortening the swing phase time, the step height of the robot was reduced while walking. This is due to the fact that the robot's shorter swing phase allows its leg to spend less time in the air and limits the robot's ability to reach a higher position before initiating its next step. Since a shorter swing phase allows the leg spends less time in the air, which limits its ability to reach a higher position before initiating the next step, it is found that shortening the swing phase duration can lead to a lower step height.

Measured tension values of all forelimb and hindlimb legs of the musculoskeletal quadruped robot in two experimental conditions, which are Gait Cycle-1 and Gait Cycle-2, are shown in Fig.5.7 and Fig.5.8, respectively. Considering the Gait Cycle-1 and Gait Cycle-2 conditions, in the second condition, an increase in tension in the forelimbs and hindlimbs was seen in the late stance phase, indicating that there was a kick with greater force happening at that moment. The late stance phase showed increased tension in the fore and hind legs, indicating a stronger kick at that moment. During the robot's walking, the legs produced a stronger kick in the second case, allowing the robot to complete the 2-meter experiment path faster than in the first condition. Therefore, this result also proves that the speed of the robot increased in the condition of Gait Cycle-2 in Fig.5.3.

Tension values of the right hindlimb, left hindlimb, right forelimb, and left forelimb of the quadruped robot under the Gait Cycle-1 condition are demonstrated in Fig.5.9, Fig.5.10, Fig.5.11, and Fig.5.12, respectively. Furthermore, tension values of right hindlimb, left hindlimb, right forelimb, and

left forelimb of the quadruped robot under the Gait Cycle-2 condition are shown in Fig.5.13, Fig.5.14, Fig.5.15, and Fig.5.16, respectively. As found in Fig.5.7 and Fig.5.8, an increase in tension is also observed in the Fig.5.9, Fig.5.10, Fig.5.11, and Fig.5.12 under the Gait Cycle-1 condition during the late stance phase and in Fig.5.13, Fig.5.14, Fig.5.15, and Fig.5.16 under the Gait Cycle-2 condition during the late stance phase. This suggests that although the tension sensor is not directly involved in the control of the robot, there is a relationship between the sensor measurement and the speed of the robot depending on the muscle model.

Figure 5.1: A snapshot of one cycle of quadruped robot in Gait Cycle-1 experiment

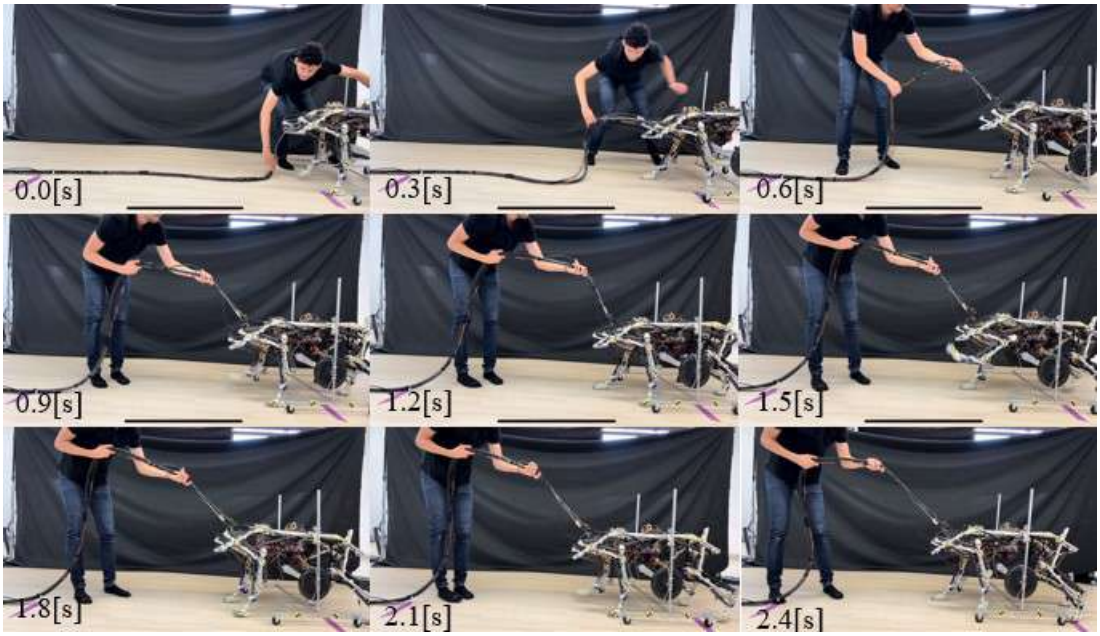

Figure 5.2: A snapshot of one cycle of quadruped robot in Gait Cycle-2 experiment

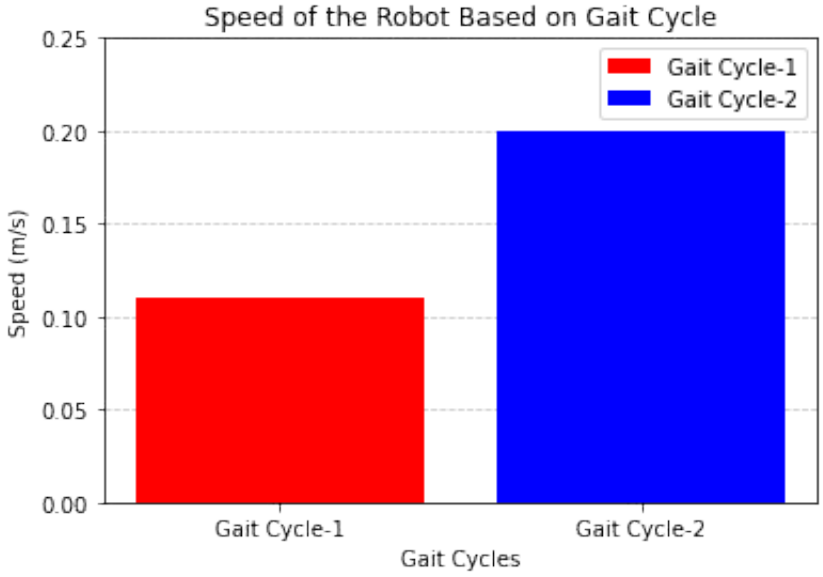

Figure 5.3: The speed of quadruped robot under Gait Cycle-1 and Gait Cycle-2 conditions

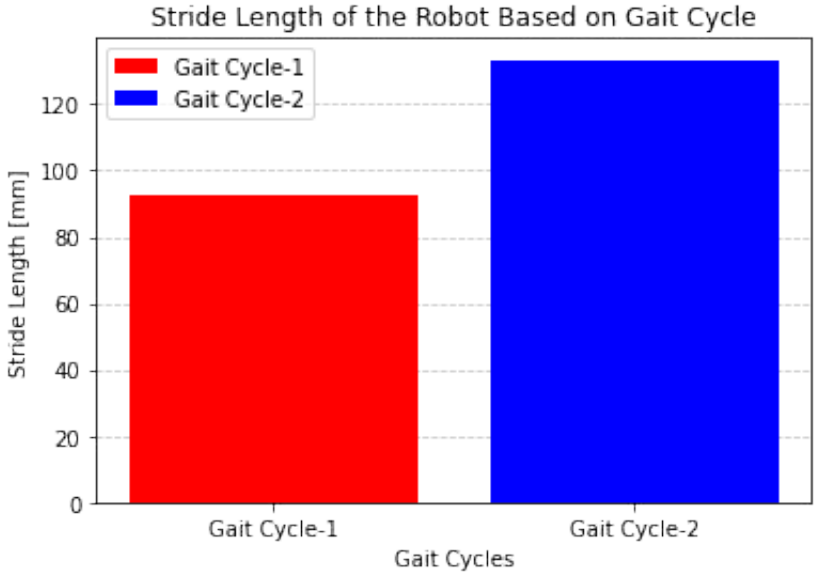

Figure 5.4: The stride length of quadruped robot under Gait Cycle-1 and Gait Cycle-2 conditions

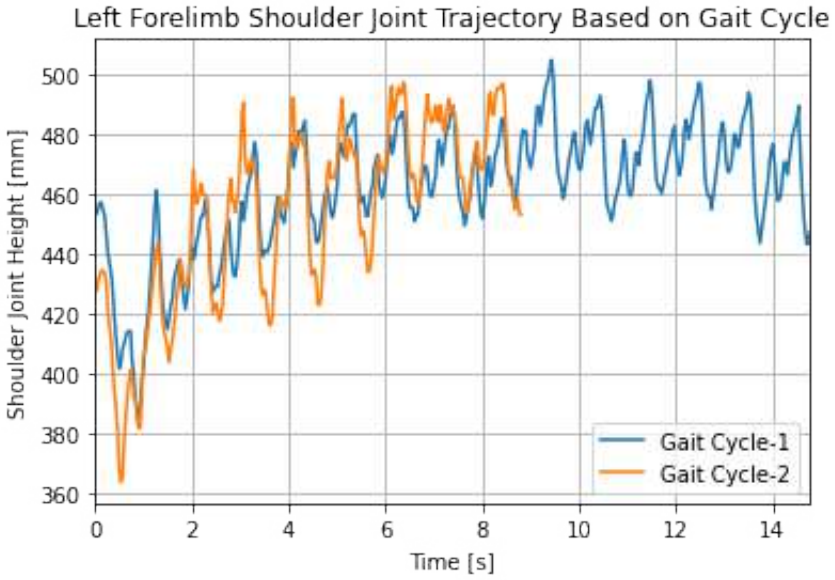

Figure 5.5: left shoulder joint trajectories under Gait Cycle-1 and Gait Cycle-2 conditions

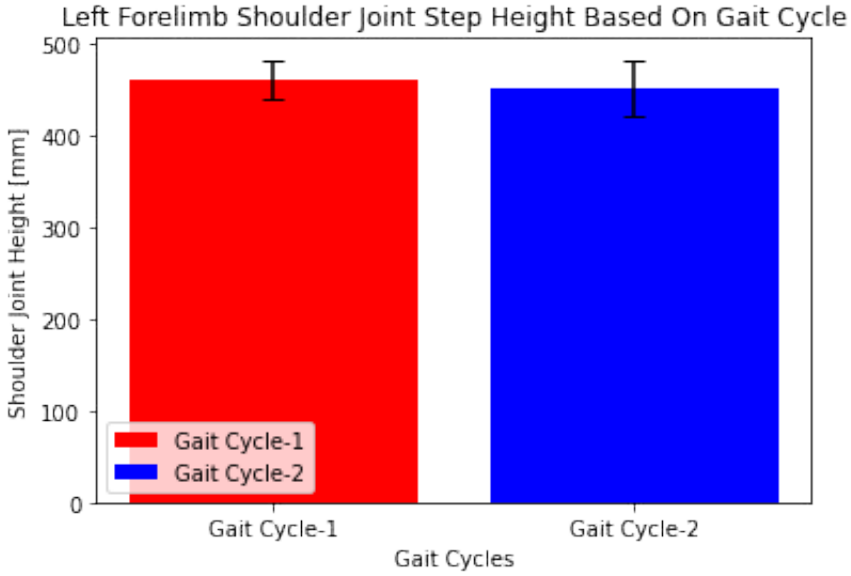

Figure 5.6: The left forelimb shoulder joint step height of the quadruped robot under Gait Cycle-1 and Gait Cycle-2 conditions

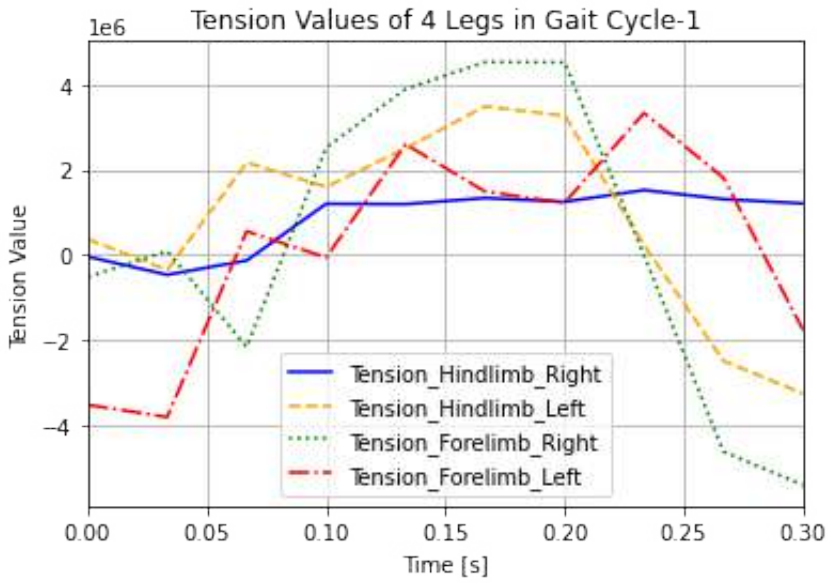

Figure 5.7: The tension values of 4 legs of the quadruped robot under Gait Cycle-1 condition

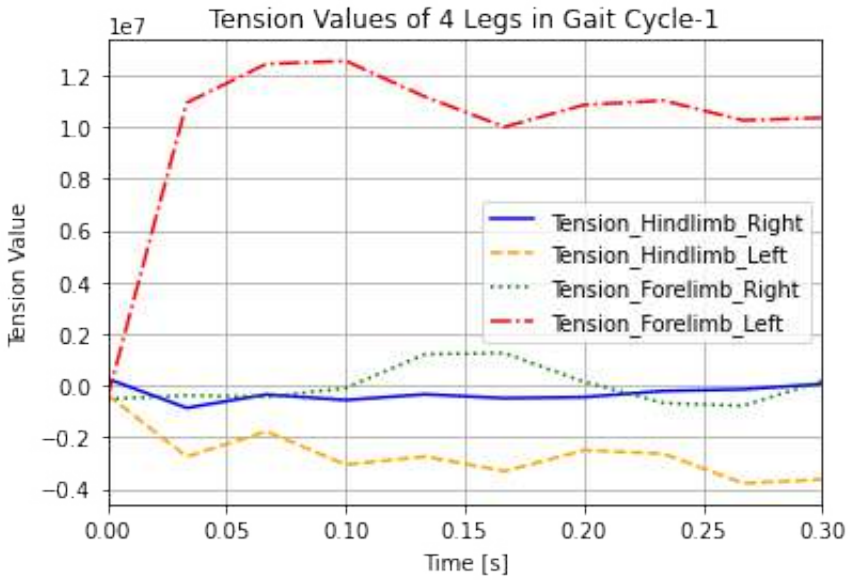

Figure 5.8: The tension values of 4 legs of the quadruped robot under Gait Cycle-2 condition

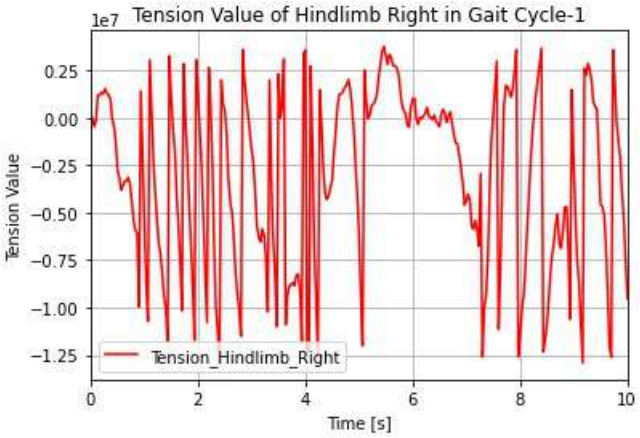

Figure 5.9: The tension values of the right hindlimb of the quadruped robot under Gait Cycle-1 condition

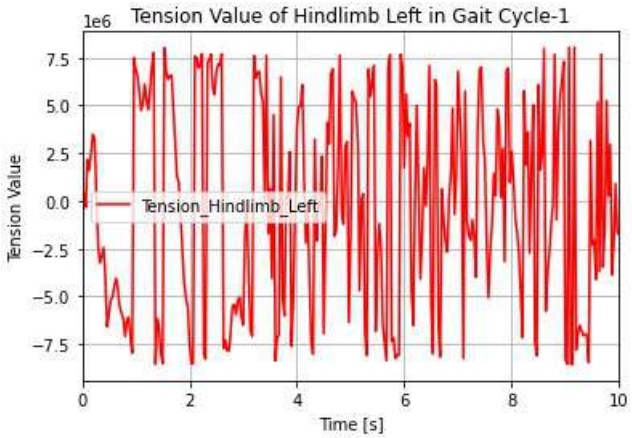

Figure 5.10: The tension values of the left hindlimb of the quadruped robot under Gait Cycle-1 condition

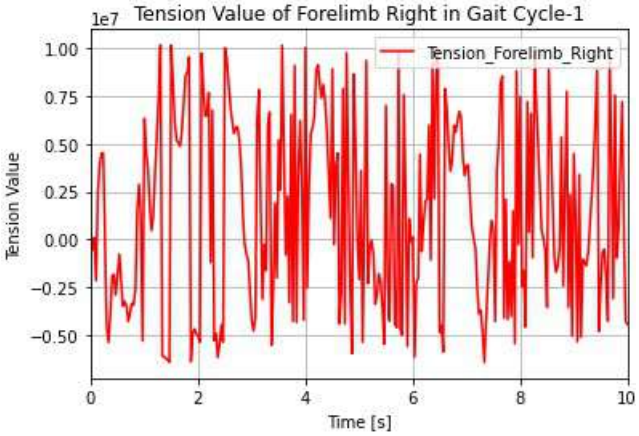

Figure 5.11: The tension values of the right forelimb of the quadruped robot under Gait Cycle-1 condition

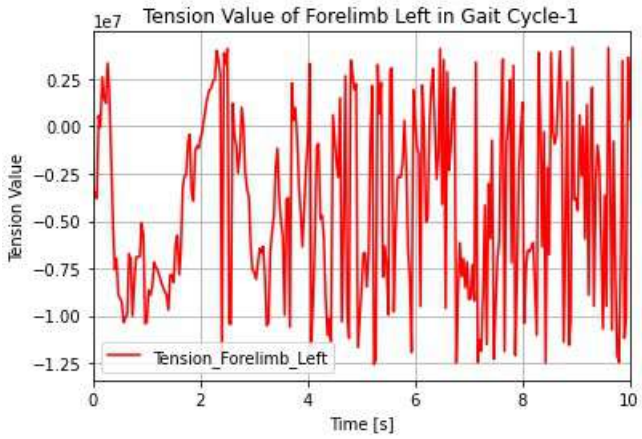

Figure 5.12: The tension values of the left hindlimb of the quadruped robot under Gait Cycle-1 condition

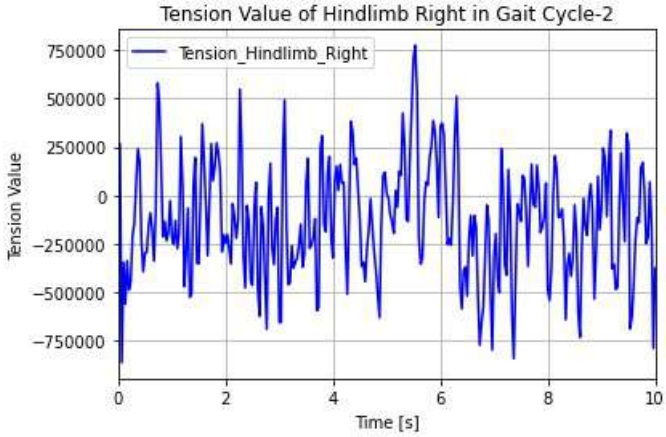

Figure 5.13: The tension values of the right hindlimb of the quadruped robot under Gait Cycle-2 condition

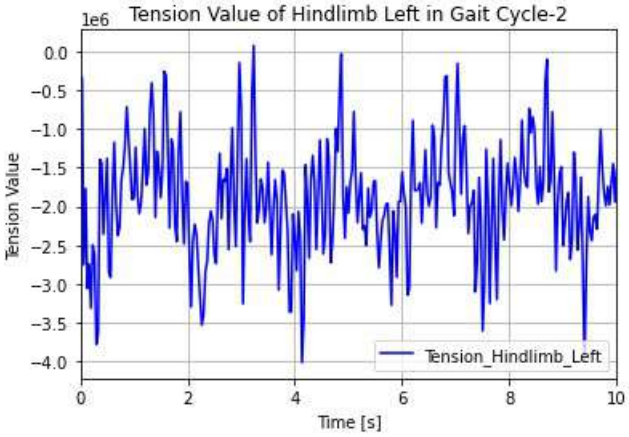

Figure 5.14: The tension values of the left hindlimb of the quadruped robot under Gait Cycle-2 condition

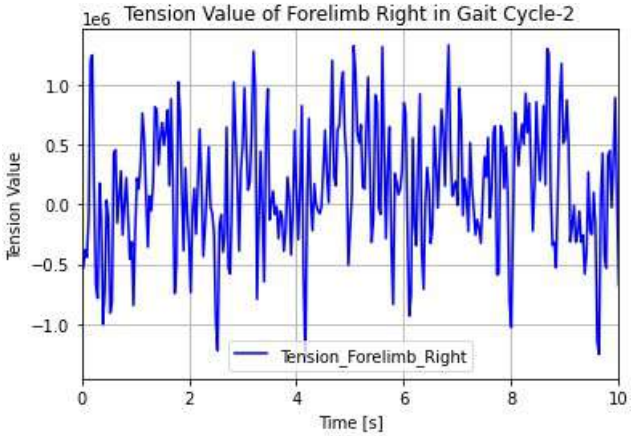

Figure 5.15: The tension values of the right forelimb of the quadruped robot under Gait Cycle-2 condition

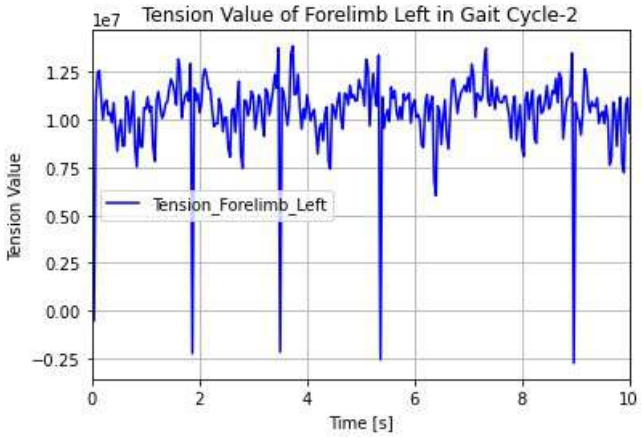

Figure 5.16: The tension values of the left hindlimb of the quadruped robot under Gait Cycle-2 condition

Chapter 6

Discussion

According to experimental results, Fig.5.3 represents that the adjustments made to the muscle pattern and the gait cycle enabled the robot to increase its speed almost twice. This proves our hypothesis stated in the proposed method and shows that reducing the duration of the stance phase and swing phase increases the speed of the robot. By reducing the stance phase duration, the robot spent less time on the ground with each leg before going into the swing phase, allowing the robot to reach a higher stride frequency. In addition, by reducing the swing phase duration, the robot spent less time in the air between steps, allowing for quicker transitions to the next step and more forward movement.

Moreover, Fig.5.4 proves that decreasing the duration time of the stance phase in the gait cycle allowed the legs to travel a greater distance with each stride and increased stride length. Increasing the stride length generally led to an increase in the robot's walking speed. With each step covering a greater distance, the robot achieved a higher overall speed within a fixed time frame. In addition, it was observed that there is an inverse relationship between stride length and swing phase duration. As the stride length increased, the time spent in the swing phase decreased. Shorter swing phases, linked to longer stride lengths, contributed to faster walking speed. This is because the robot spent less time in the air between steps, allowing for quicker transitions to the next step and more forward movement. Therefore, it was found that by increasing the stride length of the robot, the walking speed of the robot was increased.

Furthermore, based on Fig.5.5 and Fig.5.6, it was proven that by shortening the swing phase time, the step height of the robot was reduced while walking. This is due to the fact that the robot's shorter swing phase allows its leg to spend less time in the air and limits the robot's ability to reach a higher position before initiating its next step. Since a shorter swing phase

allows the leg spends less time in the air, which limits its ability to reach a higher position before initiating the next step, it is found that shortening the swing phase duration can lead to a lower step height. Therefore, it was also found that by decreasing the step height of the robot, the walking speed of the robot was increased.

In Fig.5.7 and Fig.5.8, an increase in tension value in the forelimbs and hindlimbs was found in the late stance phase, indicating that there was a kick with greater force happening at that moment. The late stance phase showed increased tension in the fore and hind legs, indicating a stronger kick at that moment. During the robot's walking, the legs produced a stronger kick in the second case, allowing the robot to complete the 2-meter experiment path faster than in the first condition. Therefore, this result also proves that the speed of the robot increased in the condition of Gait Cycle-2 in Fig.5.3.

In addition, an increase in tension value is also found in Fig.5.9, Fig.5.10, Fig.5.11, and Fig.5.12 under the Gait Cycle-1 condition during the late stance phase and in Fig.5.13, Fig.5.14, Fig.5.15, and Fig.5.16 under the Gait Cycle-2 condition during the late stance phase. This tension value increase indicates that there was a kick with greater force happening at that moment of the late stance phase. Thus, it has been suggested that there is a relationship between the tension sensor measurement and the robot speed, depending on the muscle drive pattern and the phase duration of the gait cycle, even when the tension sensor is not directly involved in the robot control.

Chapter 7

Conclusion

In this study, it was aimed to apply the walking strategy of a greyhound dog to a bio-inspired musculoskeletal quadruped robot, to perform the 3D walking of the robot based on muscle drive pattern, and to determine the effect of the gait cycle on the speed of the robot. Focusing on muscle drive pattern and duration of phases in the gait cycle we verified timing of gait phases and pattern of the pneumatic muscles have a crucial role in quadruped robot walking and speed.

The bio-inspired musculoskeletal quadruped robot modeled on the greyhound musculoskeletal system is developed. The solenoid valve system that supplies the compressed air to the artificial muscles of the robot was controlled by Arduino Dues, and sensor value transmission between the tension sensor and Arduino Dues was performed using CAN communication. The walking emergence system based on the control pattern of the pneumatic artificial muscles is realized and walking experiments of the quadruped robot are conducted. Various muscle drive patterns and gait cycles were implemented and compared to examine the effect of the muscle drive pattern and gait cycle on the speed of the robot while it performs the 3D walking. As a result of the experiments, it was confirmed that the 3D walking of the quadruped robot can be realized and the speed of the quadruped robot can be increased by adjusting the muscle pattern, decreasing the duration time of stance and swing phases of the gait cycle.

The adaptive 3D walking of the compliant quadruped robot was performed. The speed of the bio-inspired musculoskeletal quadruped was increased based on adjustments in muscle drive pattern, and transition conditions of the gait cycle. It was determined that the speed of the quadruped robot increased by decreasing the stance phase duration and the swing phase duration. It was also found that by increasing the stride length and decreasing the step height of the robot, the walking speed of the robot was increased.

In addition, it has been suggested that there is a relationship between the tension sensor measurement and the robot speed, depending on the muscle drive pattern and the phase duration of the gait cycle, even when the tension sensor is not directly involved in the robot control. Results obtained in this study are limited to conducting feedforward control due to the setting of the experiments, and the stable walking experiments based on feedback control, such as tension-based or force-based control, will be a future issue. In the future, based on the results obtained in this study, we would like to verify the dynamic contribution of muscle patterns that have various muscles in organisms that occur on the basis of stable walking.

Bibliography

[1] S. Rossignol, R. Dubuc, and J. P. Gossard, *Dynamic sensorimotor interactions in locomotion*, Brain research reviews, 2008.

[2] H. Kimura, I. Shimoyama, and H. Miura, *Dynamics and control of the quadruped robot: dynamic walking using redundancy of control inputs caused by multiple leg grounding*, The Japan Society of Mechanical Engineers(C part), sept, 1989.

[3] T. H. Smit, *The use of a quadruped as an in vivo model for the study of the spine – biomechanical considerations*, European spine journal, Apr, 2002.

[4] T. H. Smit, *Biomechanics of quadrupedal walking: how do four-legged animals achieve inverted pendulum-like movements?*, Journal of Experimental Biology, 2004.

[5] S. Grillner, *"Neurobiological bases of rhythmic motor acts in vertebrates*, Science, 1985.

[6] C. S. Sherrington, *Flexion-reflex of the limb, crossed extension-reflex, and reflex stepping and standing*, The Journal of Physiology, 1910.

[7] K. G. Pearson, *Generating the walking gait: role of sensory feedback*, Progress in brain research, 2004.

[8] S. Grillner, *Neural bases of goal-directed locomotion in vertebrates—an overview*, Brain research reviews, 2008.

[9] K. Takakusaki, and T. Okumura, *Neurobiological basis of controlling posture and locomotion*, Advanced Robotics, 2008.

[10] J. Duysens, and K. G. Pearson, *The role of cutaneous afferents from the distal hindlimb in the regulation of the step cycle of thalamic cats*, Experimental Brain Research, 1976.

[11] M. Dufosse, J. Macpherson, and J. Massion, *Biomechanical and electromyographical comparison of two postural supporting mechanisms in the cat*, Experimental Brain Research, 1982.

[12] H. Cruse, *What mechanisms coordinate leg movement in walking arthropods?*, Trends in neurosciences, 1990.

[13] P. E. Hudson, S. A. Corr, R. C. Payne Davis, S. N. Clancy, E. Lane, A. M. Wilson *Functional anatomy of the cheetah (Acinonyx jubatus) hindlimb.*, Journal of Anatomy, 2011.

[14] H. Cruse, *The function of the legs in the free walking stick insect, Carausius morosus*, Journal of comparative physiology, 1976.

[15] P. E. Hudson, S. A. Corr, R. C. Payne Davis, S. N. Clancy, E. Lane, A. M. Wilson *Functional anatomy of the cheetah (Acinonyx jubatus) forelimb.*, Journal of Anatomy, 2011.

[16] D. A. McVea, and K. G. Pearson, *Long-lasting memories of obstacles guide leg movements in the walking cat.*, The Journal of Neuroscience, 2006.

[17] G. E. Loeb, and J. Duysens, *Activity patterns in individual hindlimb primary and secondary muscle spindle afferents during normal movements in unrestrained cats.*,Journal of Neurophysiology, 1979.

[18] Y. Fukuoka, K. Hiroshi, and C. H. Avis, *Adaptive dynamic walking of a quadruped robot on irregular terrain based on biological concepts*, The International Journal of Robotics Research, 2003.

[19] K. Matsuoka, *Mechanisms of frequency and pattern control in the neural rhythm generators*, Biological cybernetics, 1987.

[20] G. Taga, Y. Yamaguchi, and H. Shimizu, *Self-organized control of bipedal locomotion by neural oscillators in an unpredictable environment, Biological cybernetics, 1991.*

[21] Y. Masuda, K. Miyashita, K. Yamagishi, M. Ishikawa, and K. Hosoda, Brainless running: a quasi-quadruped robot with decentralized spinal reflexes by solely mechanical devices, IEEE/RSJ International Conference on Intelligent Robots and Systems (IROS), Oct, 2020.

[22] H. Kimura, S. Akiyama, and K. Sakurama, Realization of dynamic walking and running of the quadruped using a neural oscillator, Autonomous robots, 1999.

[23] C. Maufroy, T. Nishikawa, and H. Kimura, Stable dynamic walking of a quadruped robot "Kotetsu" using phase modulations based on leg loading/unloading, IEEE International Conference on Robotics and Automation, 2010.

[24] Y.Yamada, S. Nishikawa, K. Shida, R. Niiyama, and Y. Kuniyoshi, Neural-body coupling for emergent locomotion: A musculoskeletal quadruped robot with spinobulbar model, IEEE/RSJ International Conference on Intelligent Robots and Systems, Sept, 2011.

[25] C. MAufroy, K. Hiroshi, and T. Kunikatsu, Integration of posture and rhythmic motion controls in quadrupedal dynamic walking using phase modulations based on leg loading/unloading, Autonomous Robots, 2010.

[26] H. Kimura, and Y. Fukuoka, Biologically inspired adaptive dynamic walking in an outdoor environment using a self-contained quadruped robot:'Tekken2', IEEE/RSJ International Conference on Intelligent Robots and Systems, Sept, 2004.

[27] G. Taga A model of the neuro-musculoskeletal system for human locomotion: I. The emergence of basic gait, Biological cybernetics, JUl, 1995.

[28] D. Owaki, T. Kano, K. Nagasawa, A. Tero, and A. Ishiguro Integration of posture and rhythmic motion controls in quadrupedal dynamic walking using phase modulations based on leg loading/unloading, Journal of The Royal Society Interface, Jan, 2013.

[29] A. Fukuhara, D. Owaki, T. Kano, R. Kobayashi, and A. Ishiguro, Spontaneous gait transition to high-speed galloping by reconciliation between body support and propulsion, Advanced robotics, 2018.

[30] F. Daerden, and D. Lefeber, Pneumatic artificial muscles: actuators for robotics and automation, European journal of mechanical and environmental engineering, 2002.

[31] D. G. Caldwell, G. Medrana-Cerda, and M. J. Goodwin Braided pneumatic actuator control of a multi-jointed manipulator, IEEE Systems Man and Cybernetics Conference, Oct. 1993.

[32] G. Andrikopoulos, G. Nikolakopoulos, and S. Manesis A survey on applications of pneumatic artificial muscles, 19th Mediterranean Conference on Control and Automation (MED), 2011.

[33] S. B. Williams, A. M. Wilson, J. Daynes, K. Peckham, and R. C. Payne, Functional anatomy and muscle moment arms of the thoracic limb of an elite sprinting athlete: the racing greyhound (Canis familiaris), Journal of Anatomy, 2008.

[34] S. B. Williams, A. M. Wilson, L. Rhodes, J. Andrews, and R. C. Payne, Functional anatomy and muscle moment arms of the pelvic limb of an elite sprinting athlete: the racing greyhound (Canis familiaris), Journal of Anatomy, 2008.

[35] E. L. Webster, P. E. Hudson, and B. S. Channon, Comparative functional anatomy of the epaxial musculature of dogs (C anis familiaris) bred for sprinting vs. fighting, Journal of Anatomy, 2014.

[36] A. Rosendo, S. Nakatsu, K. Narioka, and K. Hosoda, Producing alternating gait on uncoupled feline hindlimbs: muscular unloading rule on a biomimetic robot, Advanced Robotics, 2014.

[37] S. Nakatsu, A. Rosendo, M. Shimizu, and K. Hosoda, Realization of three-dimensional walking of a cheetah-modeled bio-inspired quadruped robot, 2014 IEEE international conference on robotics and biomimetics (ROBIO 2014), 2014.

[38] O. Ekeberg, and K. Pearson Computer simulation of stepping in the hind legs of the cat: an examination of mechanisms regulating the stance-to-swing transition, Journal of Neurophysiology, 2005.

[39] G. H. Wenting, The action of the hind limb musculature of the dog in walking, Cells Tissues Organs, 1976.

[40] G. E. Goslow, H. J. Seeherman, C. R. Taylor, M. N. McCutchlun, and N. C. Heglund, Electrical activity and relative length changes of dog limb muscles as a function of speed and gait, Journal of Experimental Biology, 1981.

[41] M. H¿ Raibert, Legged robots that balance, MIT press, 1986.